Nonequilibrium size distributions of fluid membrane vesicles

Leonardo Golubović and Mirjana Golubović
Department of Physics, West Virginia University, Morgantown, West Virginia 26506
(Received 26 December 1996)

We investigate nonequilibrium behavior of polydisperse ensembles of fluid membrane vesicles by means of a diffusive Boltzmann transport equation that incorporates vesicle diffusion and reactions between vesicles. This approach is used to study time evolutions of size distributions of initially monodisperse vesicle ensembles. We investigate various nonequilibrium paths that ensembles of vesicles may follow during the equilibration process. Depending on the initial size distribution of vesicles, the thermodynamic equilibrium may be reached either via a fusional growth of vesicles, or via their fissional decay. In the former case, typical vesicle size grows as $R(t)\sim t^{1/2}$ until it saturates to its equilibrium value, whereas in the latter case we find that vesicle size decays in a *finite time* proportional to $[R(0)]^{1/3}$, where $R(0)$ is the initial vesicle size. The latter behavior is related to the length scale dependence of membrane bending and saddle splay rigidity.
[S1063-651X(97)03109-7]

PACS number(s): 68.15.+e, 05.40.+j, 82.70.Kj

I. INTRODUCTION

In recent years significant attention has been devoted to the equilibrium statistical mechanics of fluid membranes [1], and their phases [2–8]. However, many interesting phenomena involving membranes are nonequilibrium in nature. A technologically important example are liposomes, which are potential vehicles for transporting therapeutic and diagnostic agents [9–11]. They are vesicles formed by bilayers containing amphiphilic substances such as phospholipids dispersed in water. Vesicles such as liposomes frequently have *nonequilibrium* size distributions that evolve due to reactions between vesicles. During storage, these reactions cause subsequent changes in the vesicles' sizes and thus affect their internal aqueus volume (''encapsulated volume''). On the other side, in *equilibrium*, unilamellar vesicles may form isotropic, liquidlike polydisperse *droplet phases*, in which polydispersity properties have been recently investigated experimentally by Hervè *et al.* [12], and theoretically [5–8]. These are so-called entropically stabilized vesicles, with the standard Helfrich-Evans membrane curvature free energy,

$$F=\int dS\left[\frac{\kappa}{2}H^2+\overline{\kappa}G\right], \tag{1.1}$$

where H and G are, respectively, membrane mean and Gaussian curvature, and κ and $\overline{\kappa}$ are membrane bending and saddle splay rigidity. Here we investigate various nonequilibrium paths to reach the thermodynamic equilibrium in these vesicle phases starting from a nonequilibrium, monodisperse distribution of vesicle sizes. We investigate nonequilibrium behavior of polydisperse ensembles of fluid membrane vesicles by means of a diffusive Boltzmann transport equation that incorporates vesicle diffusion and reactions between vesicles. This approach is used to study time evolutions of vesicle size distributions and their interesting properties such as the internal aqueous, encapsulated volume. We identify several types of possible nonequilibrium behaviors. Depending on the initial size distribution of vesicles, the thermodynamic equilibrium may be reached either via a fusional growth of vesicles, or via their fissional decay. In the former case, typical vesicle size grows as $R(t)\sim t^{1/2}$ until it saturates to its equilibrium value, whereas in the latter case we find that vesicle sizes decay in a *finite time* proportional to $[R(0)]^{1/3}$, where $R(0)$ is the initial vesicle size. The latter behavior is related to the length scale dependence of membrane bending and saddle splay rigidity [13]. Here we study, primarily, the situations in which a liquidlike, dilute unilamellar vesicle phase is reached at long times in the equilibrium [12]. We address also the situations in which one goes from a monodisperse state of unilamellar vesicles in which the phosphopolipid amount *exceeds* the critical value for the transition, into a lamellar fluid membrane phase. Such a unilamellar vesicle state eventually evolves into a lamellar phase (or into long lived metastable states of multilamellar vesicles [14]).

The layout of this paper is as follows. In Sec. II we formulate our transport equation and discuss its general properties. In Sec. III, we discuss various nonequilibrium paths to thermodynamic equilibrium starting from an initially monodisperse ensemble of vesicles. In Sec. IV we discuss our results and related experimental work. Some important details are discussed in the Appendices A and B.

II. TRANSPORT EQUATION FOR REACTING VESICLES

A dilute nonequilibrium polydisperse ensemble of nearly spherical unilamellar vesicles can be described by a vesicle density $\rho(A,\mathbf{x},t)$, such that $\rho(A,\mathbf{x},t)dAd^3x$ is the number of vesicles with area $A=4\pi R^2$ in the interval $(A,A+dA)$ contained in a volume element d^3x. A vesicle of area A is free to diffuse and undergo fusions with other vesicles or to split into smaller vesicles. Thus, the vesicle ensemble is a diffusion-reaction system where reactions are vesicle fusion and fission processes (see Fig. 1) preserving the total area of the vesicles (i.e., total amount of the membrane material). Here we are primarily interested in dilute vesicle states (''droplet gasses'') in which the encapsulated volume fraction is much smaller than 1. Thus, the time evolution of $\rho(A,\mathbf{x},t)$ can be described by a diffusive Boltzmann trans-

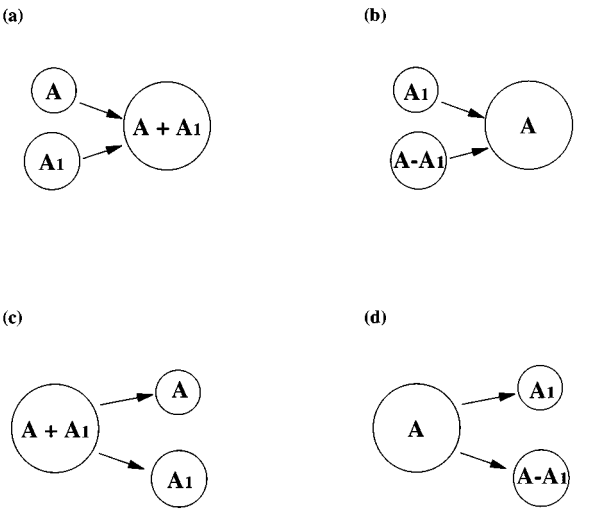

FIG. 1. Reactions between vesicles corresponding to the terms R_a to R_d of the transport equation (2.1).

port equation (TE) of the form

$$\frac{\partial}{\partial t}\,\rho(A,\mathbf{x},t)=D(A)\Delta_{\mathbf{x}}\rho(A,\mathbf{x},t)+R_a(\rho)+R_b(\rho)+R_c(\rho)+R_d(\rho), \tag{2.1}$$

where the first term is an ordinary diffusion term with the size dependent diffusion constant $D(A)=k_BT/6\pi\eta(A/4\pi)^{1/2}$, according to the Einstein-Stokes law, with η the viscosity of the solvent. R_a to R_d in Eq. (2.1) are reaction terms associated with the reactions in Fig. 1 [fusions (a) and (b), and fissions (c) and (d)]. If $\rho(A,\mathbf{x},t)$ is slowly varying in space, these terms can be generally written in the form

$$R_a(\rho)=-2\int_0^\infty dA_1\;\Gamma(A_1,A)\rho(A_1,\mathbf{x},t)\rho(A,\mathbf{x},t), \tag{2.2a}$$

$$R_b(\rho)=\int_0^A dA_1\;\Gamma(A_1,A-A_1)\rho(A_1,\mathbf{x},t)\rho(A-A_1,\mathbf{x},t), \tag{2.2b}$$

$$R_c(\rho)=2\int_0^\infty dA_1\;\Pi(A_1,A)\rho(A+A_1,\mathbf{x},t), \tag{2.2c}$$

$$R_d(\rho)=-\int_0^A dA_1\;\Pi(A_1,A-A_1)\rho(A,\mathbf{x},t). \tag{2.2d}$$

Reaction kernels Γ and Π in Eqs. (2.2) are related by the detailed balance between fusions in Fig. 1(a) and fissions in 1(c) [fusions in (b) and fissions in (c)] in the thermodynamic equilibrium. This gives the condition

$$\Pi(A_1,A_2)=\frac{\rho_{\rm eq}(A_1)\rho_{\rm eq}(A_2)}{\rho_{\rm eq}(A_1+A_2)}\,\Gamma(A_1,A_2), \tag{2.3}$$

where $\rho_{\rm eq}(A)$ is the equilibrium density. For example, for the *entropically stabilized* vesicles [5,6]

$$\rho_{\rm eq}(A)=\frac{C}{A^{5/2}}\left(\frac{A}{A_{\rm min}}\right)^{4/3}e^{-A/A_{\rm eq}}, \tag{2.4}$$

whereas $\rho_{\rm eq}(A)\approx 0$ for $A<A_{\rm min}$. Here $A_{\rm min}$ is the area of the minimum-size vesicles [6]. Dimensionless constant C in Eq. (2.4) is

$$C=\text{const}\times\left(\frac{\kappa}{k_BT}\right)^2\exp\left[-\frac{E(A_{\rm min})}{k_BT}\right], \tag{2.4$'$}$$

where $E(A_{\rm min})=8\pi\kappa+4\pi\overline{\kappa}$ is the curvature free energy of the minimum-size vesicles [6]. At low enough T, for $-2\kappa<\overline{\kappa}$ (as assumed hereafter), $C\ll 1$. The power-law prefactor $(A/A_{\rm min})^{4/3}$ in $\rho_{\rm eq}$ of Eq. (2.4) arisis from the dependence of the membrane curvature rigidities κ and $\overline{\kappa}$ on vesicle size [13]. The prefactor $A^{-5/2}$ in Eq. (2.4) originates from the entropy of vesicle's collective modes [5,6]. $A_{\rm eq}$ in Eq. (2.4) is, effectively, the area of the largest vesicles present in the system. It is determined by the total amount of the membrane material, i.e., total membrane area

$$A_{\rm tot}=\int d^3x\;dA\;A\rho(A,\mathbf{x},t) \tag{2.5}$$

present in the system. Vesicle fusion and fission processes included in our TE (2.1) preserve $A_{\rm tot}$ and drive the density $\rho(\mathbf{x},A,t)$ towards the equilibrium density (2.4) at long times. We remark that the actual value of $A_{\rm eq}$ in Eq. (2.4) does not explicitly enter the TE (2.1) [see Eqs. (2.3) and (2.4)].

To close the transport theory, we now discuss the form of the reaction kernel Γ in Eqs. (2.2). To this end, consider the process in Fig. 1(a), represented by the rate in Eq. (2.2a). The quantity $\Gamma(A_1,A)\rho(A_1)dA_1$ is the inverse of the average time $t(A_1,A)$ it takes for a vesicle of area A to encounter vesicles with areas in the interval (A_1,A_1+dA_1) and fuse with one of them. Let us first estimate the number of these encounters $N(t)$ during the time interval t. During an encounter, the vesicles are as close as $R+R_1=(\sqrt{A}+\sqrt{A_1})/(4\pi)^{1/2}$. Thus, $N(t)=V(t)\rho(A_1)dA_1$, where $V(t)$ is the volume swept in space by a sphere of radius $R+R_1$ diffusing with the diffusion constant $D(A,A_1)=D(A)+D(A_1)$ (''relative'' diffusion constant for the diffusion of A_1 in the reference frame comoving with A). The volume $V(t)$ can be estimated as $V(t)\approx(4\pi/3)(R+R_1)^3(t/t_1)$, where $t_1=(R+R_1)^2/2D(A,A_1)$ (the time it takes for the sphere to diffuse over the distance equal to its radius). Thus, $N(t)\approx(R+R_1)D(A,A_1)t\rho(A_1)dA_1$ is the number of the encounters of the vesicle of area A with vesicles with areas in the interval (A_1,A_1+dA_1). If $p_{\rm fus}$ is the probability that an encounter between the vesicles leads to a fusion, the average time $t(A_1,A)$ it takes for a fusion to occur satisfies $p_{\rm fus}N(t(A_1,A))\approx 1$. By using this, and $\Gamma(A_1,A)\rho(A_1)dA_1=1/t(A_1,A)$, we find that $\Gamma(A_1,A)\approx p_{\rm fus}[D(A_1)+D(A)](R_1+R)$. By using here the Einstein-Stokes form for $D(A)$, we find

$$\Gamma(A_1,A)\approx p_{\rm fus}\,\frac{k_BT}{\eta}\left[2+\left(\frac{A}{A_1}\right)^{1/2}+\left(\frac{A_1}{A}\right)^{1/2}\right]. \tag{2.6}$$

This equation completes our transport theory, Eqs. (2.1) to (2.6). It describes dynamics of dilute ensembles of vesicles for which the encapsulated volume fraction,

$$\Phi_V(\mathbf{x},t)=\frac{1}{3(4\pi)^{1/2}}\int dA\ A^{3/2}\rho(A,\mathbf{x},t), \qquad (2.7)$$

is small. We may thus study equilibration processes in which the dilute equilibrium vesicle phase is reached at long times. Moreover, as discussed in Sec. III, we can also address interesting situations in which one starts from a dilute ($\Phi_V<1$) monodisperse state of unilamellar vesicles in which the phosphopolipid amount *exceeds* the critical value for the transition into a lamellar fluid membrane phase [12]. Such unilamellar vesicle states eventually evolve into the lamellar phase (or into long lived metastable states of multilamellar vesicles).

Thus, we are here interested in situations in which the equilibrium state reached at long times is either the droplet (dilute vesicle) phase or the lamellar phase. This corresponds to the so-called ''droplet regime'' of the fluid membrane phase diagram [7,8]. This regime occurs for the saddle-splay (Gaussian) rigidity constant $\overline{\kappa}$ in the range $-2\kappa<\overline{\kappa}<-\frac{10}{9}\kappa$ [7,8]. In the droplet regime, the cutoff area scale $A_{\rm eq}$ in Eq. (2.4) reaches its maximum value

$$(A_{\rm eq})_{\rm max}\approx\frac{A_{\rm min}}{C^{3/4}} \qquad (2.8)$$

at the transition from the droplet to the lamellar phase [7,8]. At this transition, the encapsulated volume fraction is of the order of one (close packing of spheres). In the droplet regime, the formation of passages between droplets is, generally, energetically disfavored. Likewise, formation of droplets with nonspherical, multiply connected topologies is disfavored in the droplet regime. This regime involves phases with simple membrane topologies such as the droplet and the lamellar phase. On the other hand, beyond the present work is the so-called ''passage regime,'' which occurs for the saddle-splay rigidity constant $\overline{\kappa}$ in the range $-\frac{10}{9}\kappa<\overline{\kappa}<0$ [7,8]. There passage formation and nonspherical membrane topologies are energetically favored. This yields more complex phase equilibria involving, in addition to the lamellar and droplet phase, complex states such as infinite periodic minimal surfaces and sponge phases.

Various complex processes involved during the fusion of two vesicles are all absorbed into a single reaction constant $p_{\rm fus}$ in Eq. (2.6). Membrane fusion has the character of a nucleation process whose rate is limited by a nucleation energy barrier E_b, i.e., $p_{\rm fus}\sim\exp(-E_b/k_BT)$. Fusion involves formation of complex *nonbilayer* intermediates that eventually yield formation of a small passage (catenoidal neck) connecting vesicles (as recently reviewed in Ref. [15]). The actual nucleation transition state (i.e., the transition saddle point in the energy landscape) is, most likely, a nonbilayer intermediate state of the fusion. It is thus hard to simply relate the energy barrier E_b to common bilayer parameters such as the elastic constants κ and $\overline{\kappa}$. Nonetheless, as membrane fusion eventually yields formation of a bilayer structure involving two vesicles connected by a small passage with an energy $E_{\rm pass}$, the inequality $E_b>E_{\rm pass}$ must apply. $E_{\rm pass}$ can be estimated from the standard Helfrich-Evans elastic model (1.1) yielding $E_{\rm pass}\approx-4\pi\overline{\kappa}$ if the passage neck radius is much smaller than the vesicle size [16]. Thus, within the standard model (1.1), $E_{\rm pass}\approx4\pi|\overline{\kappa}|$ for $\overline{\kappa}<0$. However, as the typical neck radius is small for passages just emerging from vesicle fusion, the standard curvature energy model (1.1) should be corrected here by higher order terms in powers of curvatures [16,17]. These energy corrections are likely to be positive [17]. Thus $E_{\rm pass}>4\pi|\overline{\kappa}|$ for $\overline{\kappa}<0$. As $E_b>E_{\rm pass}$, one arrives at the inequality $E_b>4\pi|\overline{\kappa}|$ for $\overline{\kappa}<0$. By using this we establish an *upper bound* for the reaction constant $p_{\rm fus}\sim\exp(-E_b/k_BT)$ of the form $p_{\rm fus}<p_{\rm max}$, with

$$p_{\rm max}\sim\exp(-4\pi|\overline{\kappa}|/k_BT) \qquad (2.9)$$

for $\overline{\kappa}<0$.

We emphasize that the total membrane area (2.5) is the only conserved quantity. Other quantities, such as the number of vesicles and the encapsulated volume, change due to reactions between vesicles. We assume that these reactions are rare events (i.e., that $p_{\rm fus}$ is small) so that the time intervals between them are long enough to allow vesicles to recover nearly spherical shapes by permeation of the solvent through membranes.

Finally, we remark that the transport equation (2.1) can be put into a dimensionless, parameter-free form by introducing the dimensionless quantities $\tilde{A}=A/[A]$, $\tilde{\rho}=\rho/[\rho]$, $\tilde{t}=t/[t]$, and $\tilde{\mathbf{x}}=\mathbf{x}/[x]$, where $[A]=A_{\rm min}$, $[\rho]=C/A_{\rm min}^{5/2}$, $[t]=A_{\rm min}^{3/2}/C\Gamma_0$, and $[x]=(A_{\rm min}/Cp_{\rm fus})^{1/2}$; here $\Gamma_0=p_{\rm fus}k_BT/\eta$. This representation is convenient for presenting results obtained by numerically solving the transport equation (2.1) [see Sec. III and figures discussed therein]. By Eq. (2.4′),

$$[t]=\text{const}\times\frac{\eta k_BTA_{\rm min}^{3/2}}{\kappa^2}\,(p_{\rm fus})^{-1}\,\exp\left(\frac{4\pi(2\kappa+\overline{\kappa})}{k_BT}\right). \qquad (2.10)$$

By using the upper bound (2.9) for the reaction constant $p_{\rm fus}$ one obtains from Eq. (2.10) a *lower bound* estimate for the time scale $[t]$ of the form $[t]>[t]_{\rm min}$, with

$$[t]_{\rm min}\sim\frac{\eta k_BTA_{\rm min}^{3/2}}{\kappa^2}\exp\left(\frac{8\pi\kappa}{k_BT}\right) \qquad (2.11)$$

for $\overline{\kappa}<0$. Note that the time scale $[t]_{\rm min}$ does *not* depend on the value of the saddle-splay rigidity κ.

III. EVOLUTION OF INITIALLY MONODISPERSE VESICLES

A. Characteristic concentrations of vesicles

Here we discuss evolution of a spatially uniform, initially monodisperse ensemble of vesicles. Let n_0 be the number density of these vesicles that all, at $t=0$, initially have the same area A_0. Thus

$$\rho(A,\mathbf{x},t)\big|_{t=0}=n_0\delta(A-A_0). \qquad (3.1)$$

Here we will introduce several characteristic scales for the initial vesicle concentration n_0. The TE (2.1) will drive ρ to an equilibrium distribution of the form (2.4) with $A_{\rm eq}$ determined by the conservation of $A_{\rm tot}$, Eq. (2.5). This conservation law gives $A_{\rm eq}$ through the equation

$$\Phi_A = n_0 A_0 = \int dA\ A \rho_{\rm eq}(A) \tag{3.2}$$

(where Φ_A is membrane area per unit volume), yielding

$$A_{\rm eq} = \left(\frac{\Phi_A A_{\rm min}^{4/3}}{C} \right)^{6/5} = A_0 \left(\frac{n_0}{n_0^*} \right)^{6/5}, \tag{3.3}$$

with

$$n_0^* = \frac{C}{A_{\rm min}^{4/3}} (A_0)^{-1/6}. \tag{3.3'}$$

The volume fraction encapsulated by vesicles,

$$\Phi_V(t) = \frac{1}{3(4\pi)^{1/2}} \int dA\ A^{3/2} \rho(A,t), \tag{3.4a}$$

and the number of vesicles per unit volume,

$$n_v(t) = \int dA\ \rho(A,t), \tag{3.4b}$$

evolve from their initial values $\Phi_V(0) = [1/3(4\pi)^{1/2}] n_0 A_0^{3/2}$ and $n_v(0) = n_0$, to their equilibrium values

$$\begin{aligned} \Phi_V(\infty) &= \Phi_{V,\rm eq} \\ &= \frac{A_{\rm min}^{4/5} \Phi_A^{8/5}}{C^{3/5}} \\ &= \frac{A_{\rm min}^{4/5} (n_0 A_0)^{8/5}}{C^{3/5}} \\ &= \Phi_V(0) \left(\frac{n_0}{n_0^*} \right)^{3/5}, \end{aligned} \tag{3.5}$$

and

$$\begin{aligned} n_v(\infty) &= n_{v,\rm eq} \\ &= \frac{6C}{A_{\rm min}^{3/2}} \left[1 - \left(\frac{A_{\rm min}}{A_{\rm eq}} \right)^{1/6} \right] \\ &= \frac{6C}{A_{\rm min}^{3/2}} \left[1 - \left(\frac{C}{n_0 A_0 A_{\rm min}^{1/2}} \right)^{1/5} \right]. \end{aligned} \tag{3.6}$$

Above and hereafter, we assume that membrane area density $\Phi_A = n_0 A_0$ is well above the *critical large vesicle concentration* (clvc),

$$\Phi_{A,\rm clvc} = n_{0,\rm clvc} A_0 \approx \frac{C}{A_{\rm min}^{1/2}}. \tag{3.7}$$

This ensures that $A_{\rm eq} \gg A_{\rm min}$: note that, by Eq. (3.3),

$$\frac{A_{\rm eq}}{A_{\rm min}} \approx \left(\frac{\Phi_A}{\Phi_{A,\rm clvc}} \right)^{6/5}. \tag{3.7'}$$

Thus, for $\Phi_A > \Phi_{A,\rm clvc}$, one has, in equilibrium, large entropically stabilized vesicles with a broad, power-law distribution of sizes in the range between $A_{\rm min}$ and $A_{\rm eq}$ [see Eq. (2.4)]. For $\Phi_A > \Phi_{A,\rm clvc}$ the encapsulated volume fraction $\Phi_{V,\rm eq}$ is a *nonlinear* function of the membrane area density (i.e., surfactant volume fraction), as, by Eq. (3.5), $\Phi_V \sim \Phi_A^{8/5}$ in equilibrium. On the other hand, for $\Phi_A < \Phi_{A,\rm clvc}$ two qualitatively different situations can emerge in equilibrium: (i) If $\Phi_{A,\rm clvc} > \Phi_A > \Phi_{A,\rm cvc}$, where $\Phi_{A,\rm cvc}$ corresponds to the more common critical vesicle concentration [18], one has self-assembling of essentially monodisperse vesicles with $A \approx A_{\rm min}$. Thus, in this range of Φ_A, the volume fraction occupied by vesicles is simply proportional to the surfactant volume fraction $\Phi_V \sim \Phi_A$ in equilibrium. (ii) If $\Phi_A < \Phi_{A,\rm cvc}$ there are no vesicles present in the equilibrium. Rather, there one has isolated surfactant molecules (and, maybe, their nonbilayer aggregates).

In what follows, our primary focus will be on vesicle states that occur above the critical large vesicle concentration, $\Phi_A > \Phi_{A,\rm clvc}$. Only then one has, in thermodynamic equilibrium, strongly polydisperse vesicle size distribution of the power-law form since $\rho_{\rm eq}(A) \sim A^{-7/6}$, for A between $A_{\rm min}$ and $A_{\rm eq}$ [see Eq. (2.4)]. We remark that the encapsulated volume fraction $\Phi_{V,\rm eq} < 1$ throughout the fluidlike vesicle phase, whereas $\Phi_{V,\rm eq} \approx 1$ at the first order transition from the vesicle to the lamellar phase [7,8]. Thus, by Eq. (3.5), at the transition,

$$\Phi_{A,\rm crit} = n_{0,\rm crit} A_0 \approx \frac{C^{3/8}}{A_{\rm min}^{1/2}}, \tag{3.8}$$

whereas, by (3.7') and (3.8), $A_{\rm eq} = (A_{\rm eq})_{\rm max} = A_{\rm min}/C^{3/4}$. For a given initial vesicle size A_0, previous equations define *four* characteristic scales for the *initial* density of vesicles, n_0. They are $n_{0,\rm clvc}$ in Eq. (3.7), n_0^* in Eq. (3.3'), $n_{0,\rm crit}$ in Eq. (3.8), and $n_{v,\rm eq}$ in Eq. (3.6). Finally, as $\Phi_V(0) < 1$, one has $n_0 < n_{0,\rm max}$, where

$$n_{0,\rm max} \approx \frac{1}{A_0^{3/2}} \tag{3.9}$$

is the fifth characteristic density scale for n_0. The existence of several characteristic scales for n_0 implies the existence of several types of equilibration behaviors discussed in the following. In Fig. 2 we plot these five characteristic densities in the (A_0, n_0) plane. Note that for $A_0 > A_{\rm min}$, one has $n_{v,\rm eq} > n_0^* > n_{0,\rm clvc}$. Also note that for $A < (A_{\rm eq})_{\rm max} = A_{\rm min}/C^{3/4}$ [see Eq. (2.8)], one has $n_{0,\rm max} > n_{0,\rm crit} > n_0^*$ in Fig. 2. For any $n_0 < n_{0,\rm crit}$ the final state is the equilibrium vesicle phase. On the other hand, for n_0 in the range $n_{0,\rm crit} < n_0 < n_{0,\rm max}$, initially dilute vesicle ensembles transform, at long times, into the equilibrium lamellar phase. In this case the encapsulated volume fraction Φ_V grows, starting from an initial value smaller than 1, until it reaches the close packing limit $\Phi_V \approx 1$. At that time scale transformation into a multilamellar vesicle state occurs (as detailed below).

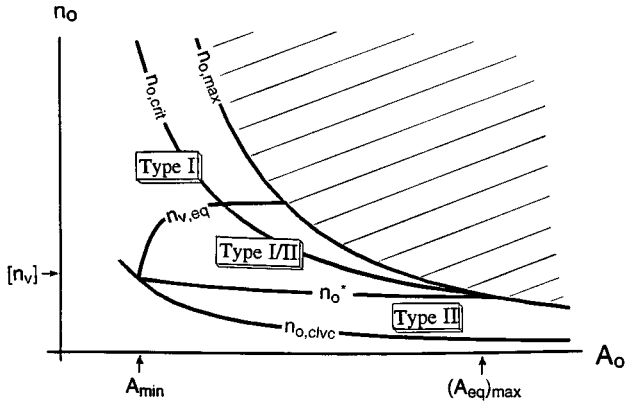

FIG. 2. Regions of the three equilibration types (I, II, and I-II) of an initially monodisperse ensemble of vesicles with the initial concentration n_0 and area A_0; here $[n_v]=C/A_{\rm min}^{3/2}$, whereas for $(A_{\rm eq})_{\rm max}$ see Eq. (2.8). Type I is above $n_{v,{\rm eq}}$, type I-II is between $n_{v,{\rm eq}}$ and n_0^*, and type II is between n_0^* and $n_{0,{\rm clvc}}$. For $n_0<n_{0,{\rm crit}}$, the final state is the dilute vesicle phase. On the other side, for n_0 in the range $n_{0,{\rm crit}}<n_0<n_{0,{\rm max}}$, initially dilute vesicle ensembles transform, at long times, into the equilibrium lamellar phase.

B. Type I equilibration

Here the initial vesicle density is above its equilibrium value, $n_0>n_{v,{\rm eq}}$. Then, also, $n_0>n_0^*$ (see Fig. 2), and, by Eqs. (3.3) and (3.5), $A_0<A_{\rm eq}$, and $\Phi_V(0)<\Phi_{V,{\rm eq}}$. Thus, the equilibration must be dominated by vesicle fusion processes [R_a and R_b terms of the TE (2.1)], which *decrease* the number density of vesicles $n_v(t)$, and, as

$$A_1^{3/2}+A_2^{3/2}<(A_1+A_2)^{3/2},$$

increase the encapsulated volume fraction $\Phi_V(t)$. This is documented in Fig. 3, obtained by numerically solving the TE (2.1) for the initial ρ in the form of a narrow Gaussian centered at A_0 (see Fig. 4 at $t=0$). We see from Fig. 3 that $\Phi_V(t)$ grows as $t^{1/2}$ until it saturates to its equilibrium value $\Phi_{V,{\rm eq}}$ at times longer than some equilibration time scale $t_{\rm eq}$. This growth can be understood analytically as, for $t\ll t_{\rm eq}$, fusional terms dominate in the TE (2.1), i.e.,

$$\frac{\partial}{\partial t}\,\rho(A,t)\approx R_a(\rho)+R_b(\rho). \tag{3.10}$$

As discussed in Appendix A, this equation has a self-similar solution of the form

$$\rho(A,t)=\frac{\Phi_A}{[A(t)]^2}\,F^*\!\left(\frac{A}{A(t)}\right) \tag{3.11}$$

[with $\int dz\; zF^*(z)=1$], characterized by a growing vesicle area scale

$$A(t)=A(0)+\Phi_A\Gamma_0 t, \tag{3.12}$$

with $\Gamma_0=p_{\rm fus}k_BT/\eta$, and $A(0)\approx A_0$. Thus, for $t\ll t_{\rm eq}$, the typical vesicle radius grows as

$$R\sim[A(t)]^{1/2}\sim t^{1/2}, \tag{3.13}$$

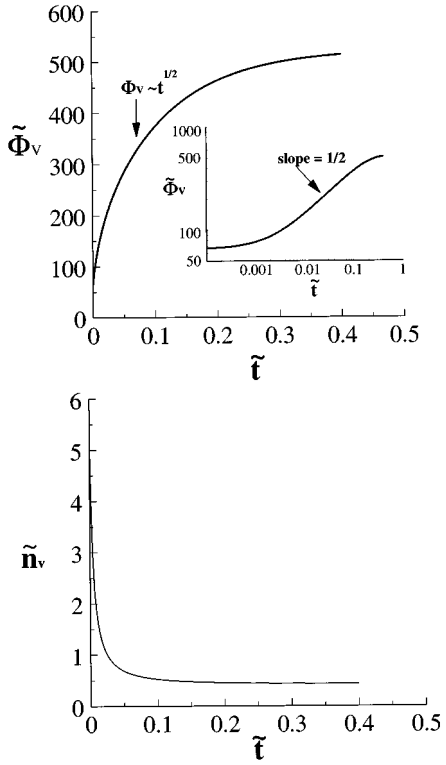

FIG. 3. Example of the type I equilibration. Here and in the following figures, $\tilde t=t/[t]$, $\tilde\Phi_V(\tilde t)=\Phi_V(t)/[\Phi_V]$, and $\tilde n_v(\tilde t)=n_v(t)/[n_v]$, with $[t]=A_{\rm min}^{3/2}/C\Gamma_0$, $[\Phi_V]=C$, and $[n_v]=C/A_{\rm min}^{3/2}$. In this example $\tilde A_0=A_0/A_{\rm min}=5$, and $\tilde n_v(0)=n_0/[n_v]=60$, whereas the initial distribution is a narrow Gaussian centered at A_0.

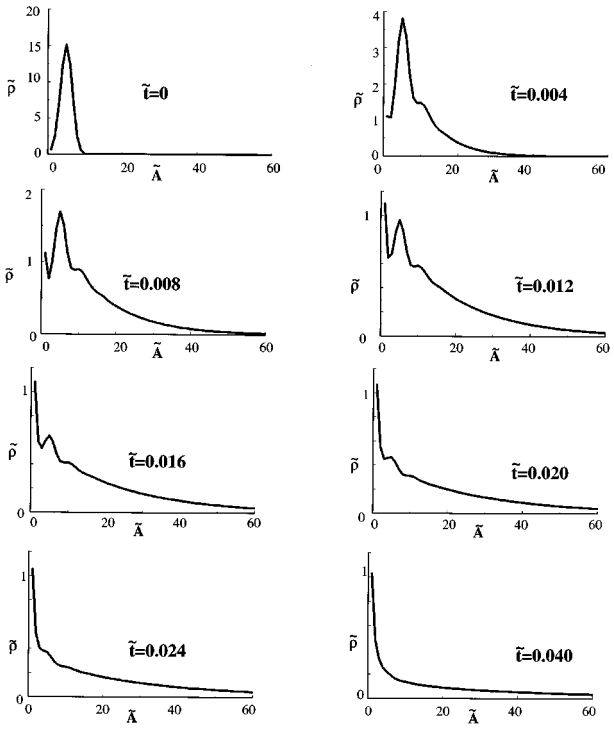

FIG. 4. For the example of the type I equilibration in Fig. 3, we plot $\tilde\rho=\rho/[\rho]$ vs $\tilde A=A/A_{\rm min}$ for various times in the interval $0<\tilde t<0.040$, early evolution. Here and in the following figures, $[\rho]=C/A_{\rm min}^{5/2}$.

whereas

$$\Phi_V(t) = \text{const} \times \Phi_A [A(t)]^{1/2} \sim t^{1/2} \tag{3.14}$$

and

$$n_v(t) = \text{const} \times \frac{\Phi_A}{A(t)} \sim t^{-1}. \tag{3.15}$$

See Appendix A. For $t \approx t_{\text{eq}}$, the area scale $A(t)$ reaches A_{eq}, $A(t_{\text{eq}}) \approx A_{\text{eq}}$, or, equivalently, $\Phi_V(t_{\text{eq}}) \approx \Phi_{V,\text{eq}}$. This, combined with Eqs. (3.12) and (3.3), yields

$$t_{\text{eq}} = \text{const} \times \frac{A_{\text{min}}^{8/5}}{C^{6/5}\Gamma_0} (\Phi_A)^{1/5}. \tag{3.16}$$

Thus,

$$t_{\text{eq}} \sim (\Phi_A)^{1/5} \sim (n_0 A_0)^{1/5} \tag{3.16'}$$

for $n_0 < n_{0,\text{crit}}$, i.e., $\Phi_A < \Phi_{A,\text{crit}}$, when the equilibrium state reached at long times is the dilute unilamellar vesicle phase (see Fig. 2). In terms of the dimensionless quantities discussed at the end of Sec. II,

$$\tilde{t}_{\text{eq}} = \frac{t_{\text{eq}}}{[t]} = \text{const} \times (\tilde{n}_0 \tilde{A}_0)^{1/5}, \tag{3.16''}$$

where $\tilde{A}_0 = A_0 / A_{\text{min}}$, and $\tilde{n}_0 = n_0 / [n_v]$, with $[n_v] = C / A_{\text{min}}^{3/2}$.

On the other hand, if the initial vesicle density $n_0 > n_{0,\text{crit}}$, the equilibrium state is the lamellar phase and vesicles will evolve via fusions until the encapsulated volume fraction becomes $O(1)$. Thus, the encapsulated volume fraction Φ_V grows, starting from an initial value smaller than 1, until it reaches the close packing limit $\Phi_V \approx 1$. At that time scale, concentrated unilamellar vesicles will transform into multilamellar long lived vesicles (corresponding to confocal defects of a smectic-*A* phase), as suggested by Simons and Cates [14]. Thus, the equilibration time scale (from dilute to concentrated vesicle state) can be estimated from $\Phi_V(t_{\text{eq}}) \approx 1$, yielding, by Eqs. (3.14) and (3.12),

$$t_{\text{eq}} = \text{const} \times \frac{1}{\Gamma_0} (\Phi_A)^{-3} \tag{3.17}$$

for $\Phi_A > \Phi_{A,\text{crit}}$. By Eqs. (3.16) and (3.17), t_{eq} has a maximum for $\Phi_A \approx \Phi_{A,\text{crit}}$, i.e., at the first order transition from the droplet to the lamellar phase at which

$$(t_{\text{eq}})_{\text{max}} \approx \frac{A_{\text{min}}^{3/2}}{C^{9/8}\Gamma_0} = \frac{[t]}{C^{1/8}}, \tag{3.18}$$

An interesting feature of the equilibration time scales t_{eq} in Eqs. (3.16) and (3.17) is that they depend on the initial vesicle density n_0 and area A_0 only through their product $n_0 A_0 = \Phi_A$.

Figures 4 and 5 give time evolution of the vesicle distribution $\rho(A,t)$ during the type I equilibration [the corresponding $\Phi_V(t)$ and $n_v(t)$ are in Fig. 3]. Figure 4 gives early evolution of $\rho(A,t)$ starting from a Gaussian centered at $A_0 = 5A_{\text{min}}$. We see that fusions quickly produce another, weaker peak at $A = 10A_{\text{min}}$. Higher order peaks (third, etc.) are smeared and not observable here. In Fig. 4 we see also the emerging peak at $A = 0$, which is produced by fissions. Fissions, however, only weakly affect the dynamics of $\Phi_V(t)$ and $n_v(t)$ for $t < t_{\text{eq}}$. Figure 5 gives evolution of $\rho(A,t)$ over a broader range of A and t. In the log-log representation of Fig. 5 it is manifest that the main changes of ρ are in the range of large A where ρ is relatively small. Still, such changes are sufficient to produce a significant variation of $\Phi_V(t)$ and $n_v(t)$ in Fig. 3 before equilibrium is reached.

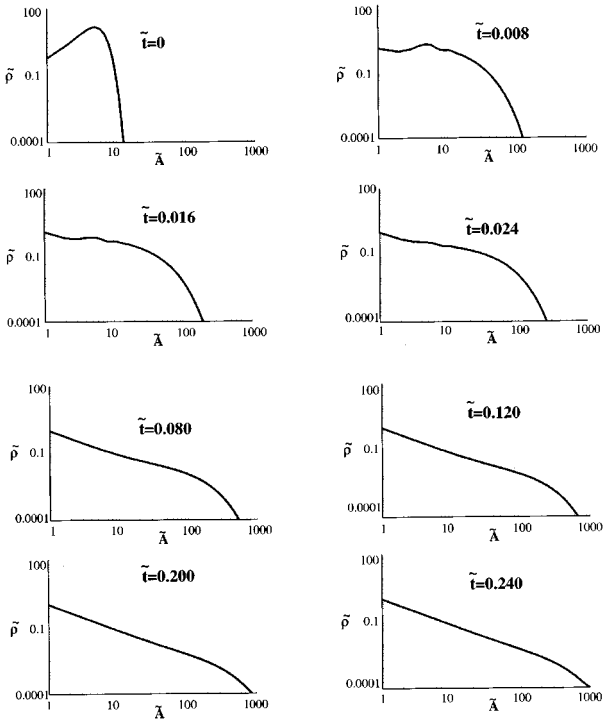

FIG. 5. The same as in Fig. 4 but in log-log scales and in the broader time interval $0 < \tilde{t} < 0.28$.

C. Type II equilibration

Here the initial vesicle density n_0 is in the range $n_{0,\text{clvc}} < n_0 < n_0^*$ (then, also, $n_0 < n_{v,\text{eq}}$, see Fig. 2). Then, by Eqs. (3.3) and (3.5), $A_0 > A_{\text{eq}}$, and $\Phi_V(0) > \Phi_{V,\text{eq}}$. Thus, the equilibration must be dominated by vesicle fission processes [R_c and R_d terms of the TE (2.1)], which increase the number density of vesicles $n_v(t)$, and, as $A_1^{3/2} + A_2^{3/2} < (A_1 + A_2)^{3/2}$, decrease the encapsulated volume fraction $\Phi_V(t)$. This is documented in Fig. 6, obtained by numerically solving the TE (2.1) [$\rho(A, t=0)$ is a Gaussian centered at A_0]. We see that $\Phi_V(t)$ decreases, whereas the vesicle density $n_v(t)$ increases, until they saturate to their equilibrium values at times longer than some equilibration time scale t_{eq}. Details of this behavior can be understood analytically as, for $t \ll t_{\text{eq}}$, fissional terms dominate in the TE (2.1), i.e.,

$$\frac{\partial}{\partial t} \rho(A,t) \approx R_c(\rho) + R_d(\rho). \tag{3.19}$$

By analyzing this equation (see Appendix B), we find that an initially monodisperse size distribution gets replaced by a transient strongly polydisperse distribution of the form

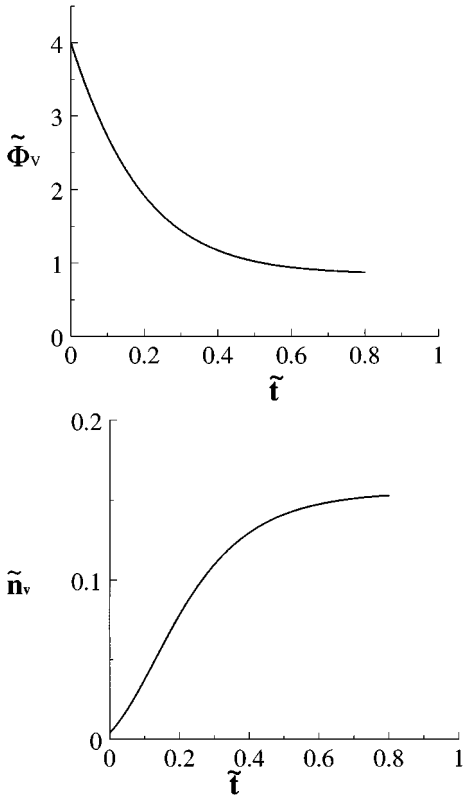

FIG. 6. Example of the type II equilibration. Here $\tilde{A}_0=100$, and $\tilde{n}_v(0)=n_0/[n_v]=0.042$, whereas the initial distribution is a narrow Gaussian centered at A_0.

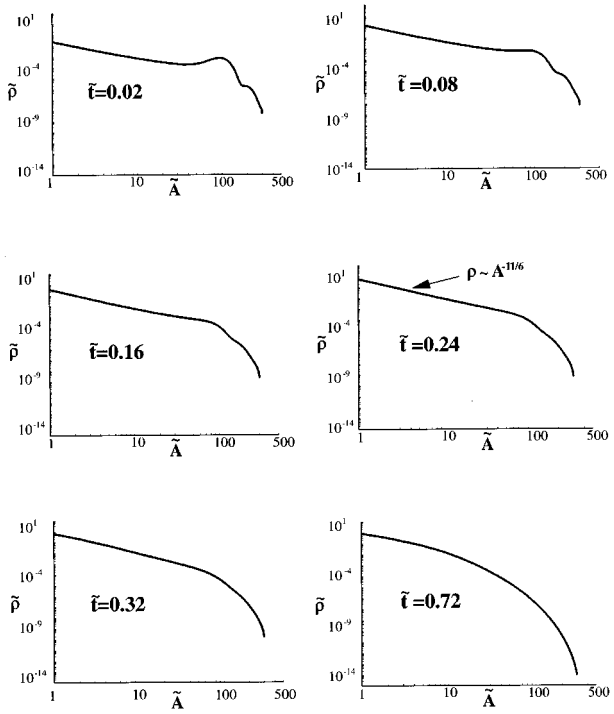

FIG. 7. For the example of the type II equilibration in Fig. 6 we give log-log plots of $\tilde{\rho}$ vs $\tilde{A}$ for various times in the interval $0<\tilde{t}<0.72$.

$$\rho \sim \frac{1}{A^{11/6}} \tag{3.20}$$

for $A<A(t)$, and $\rho \approx 0$, for $A>A(t)$. Such a transient behavior of $\rho(A,t)$ is documented also by the numerical solution of the TE (2.1); see Fig. 7. In Appendix B we find that the time dependent cutoff area scale $A(t)$ decays to zero as

$$A(t)=A_0\left[1-\frac{t}{t_{\rm eq}}\right]^6, \tag{3.21}$$

with

$$t_{\rm eq}=\text{const}\times\frac{A_{\rm min}^{4/3}}{C\Gamma_0}A_0^{1/6}. \tag{3.22}$$

Thus, for the type II equilibration, the equilibration time scale behaves as

$$t_{\rm eq}\sim(A_0)^{1/6}\sim(R_0)^{1/3}. \tag{3.22$'$}$$

So, the equilibration is dominated by the fissional decay of vesicles, which occurs in a *finite time* proportional to $R_0^{1/3}$, where R_0 is the initial vesicle size, as detailed in Appendix B. The above transient form of $\rho(A,t)$, Eq. (3.20), as well as the form of $t_{\rm eq}$ in Eq. (3.22), are consequences of the particular form of the equilibrium vesicle distribution $\rho_{\rm eq}(A)$, Eq. (2.4), which enters the fissional part of the TE (2.1) due to the detailed balance condition (2.3). Thus, Eqs. (3.20) to (3.22) reflect the length scale dependence of membrane bending and saddle splay rigidity on the vesicle size [13], as well as entropy of vesicle collective degrees of freedom incorporated in $\rho_{\rm eq}$, Eq. (4) [5,6]. In terms of the dimensionless quantities discussed at the end of Sec. II, Eq. (3.22) assumes the simple form

$$\tilde{t}_{\rm eq}=\frac{t_{\rm eq}}{[t]}=\text{const}\times(\tilde{A}_0)^{1/6}, \tag{3.22$''$}$$

with $\tilde{A}_0=A_0/A_{\rm min}$.

D. Type I-II equilibration

Here the initial vesicle density n_0 is between n_0^* and $n_{v,\rm eq}$ ($n_0^*<n_0<n_{v,\rm eq}$); see Fig. 2. By numerically solving the TE (2.1), we obtain $\Phi_V(t)$ and $n_v(t)$ in Fig. 8. As $n_0<n_{v,\rm eq}$, the vesicle density $n_v(t)$ increases until it saturates to $n_{v,\rm eq}$. In this respect, this equilibration is similar to type II equilibration. As there, this increase of $n_v(t)$ is produced here by the fissional terms of the TE (2.1). However, as $n_0^*<n_0$ here, one has, by Eqs. (3.3) and (3.5), $A_0<A_{\rm eq}$ and $\Phi_V(0)<\Phi_{V,\rm eq}$. Thus, the encapsulated volume fraction $\Phi_V(t)$ increases until it saturates to $\Phi_{V,\rm eq}$. In this respect, this equilibration is similar to the type I equilibration. As there, this increase of $\Phi_V(t)$ is produced here by the fusional terms of the TE (2.1). From Fig. 8, we see that the fissional increase of $n_v(t)$ produces an *overshoot* above the equilibrium value, yielding a maximum of $n_v(t)$ at some characteristic time scale t_1. For $t<t_1$, the fission produced vesicles are small, and do not significantly affect the encapsulated volume fraction, which continuously increases (see Fig. 8), due to fusions of the largest vesicles, which contribute most to Φ_V.

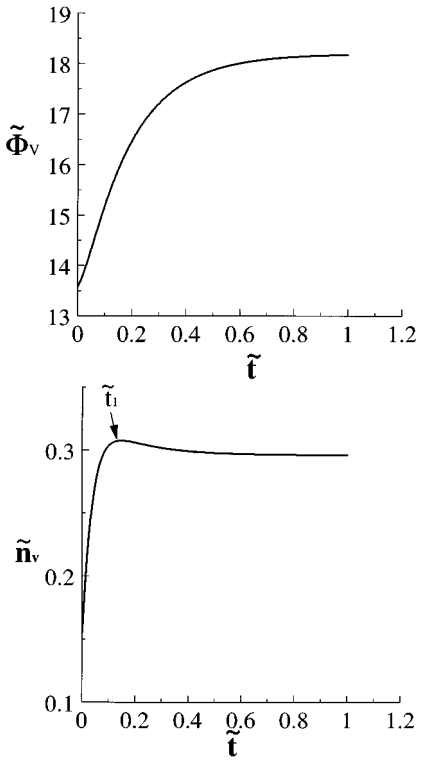

FIG. 8. Example of the type I-II equilibration. Here $\tilde{A}_0=20$ and $\tilde{n}_v(0)=1.6$, whereas the initial distribution is a narrow Gaussian centered at A_0.

Fusions, however, affect the number density of vesicles n_v significantly less. For example, after the overshoot in n_v at $t=t_1$ (Fig. 8) there is only a small decrease of $n_v(t)$, which is due to fusions of the largest vesicles in the tail of the distribution. Thus, most of the production of n_v is due to fissions and it is practically over already at the fissional time scale $t\sim t_1\approx(A_{\min}^{4/3}/C\Gamma_0)A_0^{1/6}$, as in the type II equilibration, Eq. (3.22). At this time scale, fusions still go on and increase Φ_V; see Fig. 8. Thus, the *ultimate* equilibration time $t_{\rm eq}$ is determined by fusions. $t_{\rm eq}$ is thus given by the fusional time scale $t_{\rm eq}=(A_{\min}^{8/5}/C^{6/5}\Gamma_0)(\Phi_A)^{1/5}$, as in type I equilibration, Eq. (3.16). This $t_{\rm eq}$ is larger than the fissional time scale t_1 as $t_1/t_{\rm eq}\approx(n_0^*/n_0)^{1/5}<1$ here. This applies for $n_0<n_{0,\rm crit}$ when the equilibrium state is the dilute vesicle phase. On the other hand, for $n_0>n_{0,\rm crit}$, the type I-II equilibration ends in the phase of multilamellar vesicles (see Fig. 2). In this case $t_{\rm eq}$ is given by Eq. (3.17). Thus, in general, the dependence of the equilibration time on n_0 and A_0 is the same for type I and type I-II regimes.

IV. SUMMARY AND DISCUSSION

To summarize, we investigated nonequilibrium behaviors of polydisperse ensembles of fluid membrane vesicles by means of a diffusive Boltzmann transport equation that incorporates vesicle diffusion and reactions between vesicles. This approach is used to study time evolutions of size distributions of initially dilute, monodisperse ensembles of vesicles. We identified several types of possible nonequilibrium behaviors. Depending on the initial size distribution of vesicles, the equilibration is dominated either by a fusional growth of vesicles (type I equilibration), or by their fissional decay (type II equilibration), or by a combination of both (type I-II equilibration). Here we studied, primarily, the situations in which a dilute, liquidlike dilute monolamellar vesicle phase is reached at long times in the equilibrium. We addressed also the situations in which one starts from a monodisperse state of unilamellar vesicles in which the surfactant amount exceeds the critical value for the transition into a lamellar fluid membrane phase. Such a dilute unilamellar vesicle state eventually evolves into a lamellar phase (or, in practice, into long lived metastable states of multilamellar vesicles).

Vesicle size distributions were studied in more detail in the experiments of Hervè *et al.*, both in the dilute and in the concentrated (multilamellar) regimes [12]. Interestingly, the dilute phase does not show behavior in agreement with the equilibrium size distribution (2.4), which was rigorously derived in the recent work of Morse and Milner [6]. The discrepancy between the theory and the experiment remains unresolved (see Ref. [6] for a discussion of this problem). In brief, strongly polydisperse behavior of Eq. (2.4), with $\rho_{\rm eq}\sim A^{-7/6}$, for A between $A_{\min}$ and $A_{\rm eq}$, was not observed in the experiments of Hervè *et al.* Rather, the potential $A_{\rm eq}$ appears to be only few times bigger than the observed $A_{\min}$, and the size distribution behaves, qualitatively, as a monodisperse distribution throughout the dilute vesicle phase. For example, Hervè *et al.* find $\Phi_V\sim\Phi_A$, as in a monodisperse state, rather than $\Phi_V\sim\Phi_A^{8/5}$ as in Eq. (3.5). Here we wish to suggest that the size distribution they observed in the dilute vesicle phase might not be the true equilibrium distribution. In fact, whereas the self-assembling of vesicles with $A\sim A_{\min}$ may be a fast process (above the critical vesicle concentration), the subsequent growth of large vesicles with $A\sim A_{\rm eq}$ can be a *very slow* process. This process must proceed via vesicle fusions, i.e., through the type I equilibration discussed in Sec. III. Note that the typical time scale for various equilibration types is $[t]$, Eq. (2.10) [see Eqs. (3.16″), (3.18), and (3.22″)]. In Sec. II we find that $[t]>[t]_{\min}$ with $[t]_{\min}$ given by Eq. (2.11) (for $\bar{\kappa}<0$). For $T=300$ K, Eq. (2.11) yields the practical estimate

$$[t]_{\min}\sim 10^{-2}\ \mathrm{s}\times\left(\frac{k_BT}{\kappa}\right)^2\frac{\eta}{\eta_w}\left(\frac{R_{\min}}{100\ \mathrm{nm}}\right)^3(8.22\times10^{10})^{\kappa/k_BT},\tag{4.1}$$

where η_w is the viscosity of water at 300 K and $R_{\min}$ is the radius of the minimum-size vesicles. $R_{\min}\approx20$ nm in the experiments of Hervé *et al.* [12]. Thus, for a moderately stiff membrane, with $\kappa=k_BT$, Eq. (4.1) would predict $[t]\sim10^7$ s$\sim$100 d. Hervè *et al.* suggest an even bigger $\kappa=4k_BT$, as obtained by independent measurements on oriented samples in the lamellar phase [12]. With such a κ, Eq. (4.1) would yield a value of $[t]$ exceeding many orders in magnitude the age of the Universe. If so, fusions producing large vesicles with $A\sim A_{\rm eq}$, starting from the initial vesicles with $A\sim A_{\min}$, would never occur on the experimental time scale. The waiting time for the power-law distribution $\rho_{\rm eq}\sim A^{-7/6}$ ($A_{\min}<A<A_{\rm eq}$) to develop is simply too long. Thus, on the experimental time scale, the vesicle distribution remains practically monodisperse with $A\sim A_{\min}$. In fact, this corresponds exactly to what Hervè *et al.* observe *throughout*

their dilute vesicle phase. Thus, we believe that the dilute vesicle state studied in Ref. [12] could be very far from the true equilibrium state. This explains the difference between the observations of these experiments and the theoretical predictions based on the equilibrium statistical mechanics. At least, the above discussion suggests that one should be very careful in interpreting experimental data on membrane ensembles by using results of the equilibrium theory of fluctuating surfaces. Nonequilibrium effects may dominate even in seemingly simple states such as the dilute vesicle state in which dynamics has been studied in this paper.

ACKNOWLEDGMENT

This work was supported by Mylan Laboratories.

APPENDIX A

Here we discuss the fusion-dominated diffusive Boltzmann equation

$$\frac{\partial}{\partial t}\,\rho(A,t)=R_a(\rho)+R_b(\rho), \tag{A1}$$

which is of interest for understanding the type I behavior in Sec. III. To discuss Eq. (A1), let us make the change of variables

$$\rho(A,t)=\frac{\Phi_A}{A(t)^2}\,F\left(\frac{A}{A(t)},t\right)=\frac{\Phi_A}{[A(t)]^2}\,F(z,t) \tag{A2}$$

and

$$z=\frac{A}{A(t)}. \tag{A3}$$

Here $A(t)$ is a time-dependent vesicle area scale (to be determined in the following). This change transforms Eq. (A1) into

$$A(t)\,\frac{\partial F(z,t)}{\partial t}+\frac{dA(t)}{dt}\left[-2F(z,t)-z\,\frac{\partial F(z,t)}{\partial z}\right]=\Phi_A\Gamma_0[\widetilde{R}_a(F)+\widetilde{R}_a(F)], \tag{A4}$$

with $\Gamma_0=p_{\rm fus}k_BT/\eta$, and

$$\widetilde{R}_a(F)=-2\int_0^\infty dz_1\;\widetilde{\Gamma}(z_1,z)F(z_1,t)F(z,t), \tag{A5}$$

$$\widetilde{R}_b(F)=\int_0^z dz_1\;\widetilde{\Gamma}(z_1,z-z_1)F(z_1,t)F(z-z_1,t), \tag{A6}$$

with $\widetilde{\Gamma}(z_1,z)=2+(z/z_1)^{1/2}+(z_1/z)^{1/2}$. Equation (A4) has a time-independent solution $F(z,t)=F^*(z)$, provided

$$\frac{dA(t)}{dt}=\Phi_A\Gamma_0, \tag{A7}$$

i.e.,

$$A(t)=A(0)+\Phi_A\Gamma_0 t, \tag{A8}$$

so that, by Eq. (A4), $F^*(z)$ satisfies

$$-2F^*(z)-z\,\frac{\partial F^*(z)}{\partial z}=\widetilde{R}_a(F^*)+\widetilde{R}_b(F^*). \tag{A9}$$

$F^*(z)$ yields a self-similar solution of Eq. (A1) of the form

$$\rho(A,t)=\frac{\Phi_A}{A(t)^2}\,F^*\left(\frac{A}{A(t)}\right), \tag{A10}$$

For this solution, by Eq. (A8) the typical vesicle size, $R\sim A(t)^{1/2}$, grows as $t^{1/2}$, whereas, by (A10), (3.4a), and (3.4b),

$$\Phi_V(t)=c_1\Phi_A[A(t)]^{1/2}\sim t^{1/2}, \tag{A11}$$

with $c_1=[1/3(2\pi)^{1/2}]\int dz\;z^{3/2}F^*(z)$, and

$$n_v(t)=c_2\,\frac{\Phi_A}{A(t)}\sim t^{-1}, \tag{A12}$$

with $c_2=\int dz\;F^*(z)$. In terms of the ''proper time''

$$\tau=\int_0^t dt'\;\frac{\Phi_A\Gamma_0}{A(t')}=\ln\left(1+\frac{\Phi_A\Gamma_0 t}{A(0)}\right), \tag{A13}$$

Eq. (A4) assumes the parameter-free form

$$\frac{\partial F(z,\tau)}{\partial\tau}+\left[-2F(z,\tau)-z\,\frac{\partial F(z,\tau)}{\partial z}\right]=\widetilde{R}_a(F)+\widetilde{R}_a(F), \tag{A14}$$

whose τ-independent solution satisfies Eq. (A4). Equations (A8)–(A12) explain numerical results we find in Sec. III for the type I behavior. They reflect general features of fusion-dominated behaviors as (i) there exists time-independent solution of Eq. (A14), i.e., Eq. (A9) has a solution for $F^*(z)$, and (ii) this solution is a global attractor (a universal distribution shape function) for all other solutions, e.g., initially nearly monodisperse distributions. We checked (i) and (ii) by numerically solving Eq. (A14) for the initial distributions having the form of a Gaussian peaked around a nonzero z. We find that, for large τ, $F(z,\tau)$ approaches a limiting distribution $F^*(z)$. We find that $F^*(z)$ has an exponential tail for large z, whereas it approaches a finite (nonzero) value as $z\to 0$.

APPENDIX B

Here we discuss the fission-dominated diffusive Boltzmann equation

$$\frac{\partial}{\partial t}\,\rho(A,t)=R_a(\rho)+R_b(\rho), \tag{B1}$$

which is of interest for understanding the type II equilibration behavior. Equation (B1) can be rewritten as

$$\frac{\partial}{\partial t}\,\rho(A,t)=\gamma\int_0^\infty dA'\;L(A,A')\rho(A',t), \tag{B2}$$

with $\gamma=C\Gamma_0/A_{\rm min}^{4/3}$, and

$$L(A,A') = 2\,\theta(A'-A)\,\pi(A'-A,A) - \delta(A-A')\int_0^A dA_1\,\pi(A_1,A-A_1), \quad \text{(B3)}$$

where $\theta(A'-A)$ is the step function of $A'-A$, and

$$\pi(A_1,A_2) = \left(\frac{1}{A_1}+\frac{1}{A_2}\right)^{7/6}\left[2+\left(\frac{A_1}{A_2}\right)^{1/2}+\left(\frac{A_2}{A_1}\right)^{1/2}\right]. \quad \text{(B4)}$$

The matrix $L(A,A')$ has the scaling symmetry

$$L(sA,sA') = s^{-7/6}L(A,A') \quad \text{(B5)}$$

for any s. This implies that

$$L(A,A') = A^{-7/6}\Psi\left(\frac{A'}{A}\right), \quad \text{(B6)}$$

with

$$\Psi(s) = L(1,s). \quad \text{(B7)}$$

By Eqs. (B7) and (B3), $\Psi(s)=0$ for $s<1$, and $\Psi(s)\approx s^{1/2}$ for $s\gg 1$. It is straightforward to show that

$$\int_0^\infty dA'\; L(A,A')(A')^n = f(n)A^{n-1/6} \quad \text{(B8)}$$

and

$$\int_0^\infty dA\; A^n\; L(A,A') = f(-n-\tfrac{5}{6})(A')^{n-1/6}, \quad \text{(B9)}$$

with

$$f(n) = \int_0^\infty ds\; \Psi(s)s^n. \quad \text{(B10)}$$

As $\Psi(s)\sim s^{1/2}$ for large s, $f(n)\to+\infty$ as $n\to-\frac{3}{2}$ from the left. By Eq. (B6), the fissional transport equation (B2) can be rewritten as

$$\frac{\partial}{\partial t}\,\rho(A,t) = \frac{\gamma}{A^{7/6}}\int_0^\infty dA'\Psi\left(\frac{A}{A'}\right)\rho(A',t). \quad \text{(B11)}$$

Next, consider the moments

$$m_n(t) = \int_0^\infty dA\; A^n\rho(A,t). \quad \text{(B12)}$$

By Eqs. (B9)–(B12), one obtains that

$$\frac{dm_n(t)}{dt} = \gamma f(-n-\tfrac{5}{6})m_{n-1/6}(t). \quad \text{(B13)}$$

Membrane area density $\Phi_A = m_1(t)$ is a conserved quantity. Thus, by Eq. (B13) with $n=1$,

$$f(-\tfrac{11}{6}) = 0. \quad \text{(B14)}$$

An interesting consequence of Eq. (B14) is that the fissional transport equation (B1) has a time-independent solution of the form

$$\rho(A)\sim\frac{1}{A^{11/6}} \quad \text{(B15)}$$

[see Eqs. (B2) and (B8)]. Recall that, from the numerical results in Sec. III, we saw such a behavior of ρ (see Fig. 7), but only as a transient effect in the evolution of the size distribution. In fact, ρ of the form Eq. (B15) cannot be an accessible distribution because the membrane area density $\Phi_A = m_1$ is divergent for such a distribution. Such a divergence can be removed by an upper cutoff in the integral in Eq. (B12), i.e., by a modified distribution of the form (B15) for $A<A(t)$, and $\rho(A)\approx 0$ for $A>A(t)$, where $A(t)$ as some cutoff area scale. Such a modified distribution may evolve slowly and occupy a significant part of the transient during the fission-dominated evolution. Let us explore this feature suggested by the numerical results of Sec. III. To proceed, we make the change of variables

$$\xi = A^{1/6} \quad \text{(B16)}$$

and

$$\rho(A,t) = \frac{\phi(\xi,t)}{A^{11/6}} = \frac{\phi(\xi,t)}{\xi^{11}}. \quad \text{(B17)}$$

With this change, the fissional transport equation (B11) is transformed into

$$\frac{\partial\phi(\xi,t)}{\partial t} = \frac{\gamma}{\xi}\int_0^\infty \frac{ds}{s^{11/6}}\,\Psi(s)\,\phi(s^{1/6}\xi,t). \quad \text{(B18)}$$

Equation (B18) has a simple time-independent solution in the form of a constant, $\phi(\xi,t)=\text{const}$, corresponding, by Eq. (B17), to the steady solution (B15). Furthermore, Eq. (B18) is equivalent to

$$\frac{\partial\phi(\xi,t)}{\partial t} = \gamma\int_0^\infty \frac{ds}{s^{11/6}}\,\Psi(s)\,\frac{\phi(s^{1/6}\xi,t)-\phi(\xi,t)}{\xi}, \quad \text{(B19)}$$

see Eqs. (B10) and (B14). By taking the limit $\xi\to 0$ in Eq. (B19), we obtain

$$\left.\frac{\partial\phi(\xi,t)}{\partial t}\right|_{\xi=0} = \gamma f\left(-\frac{5}{3}\right)\left.\frac{\partial\phi(\xi,t)}{\partial\xi}\right|_{\xi=0}. \quad \text{(B20)}$$

Let us consider the moments of $\phi(\xi,t)$:

$$M_\alpha(t) = \int_0^\infty d\xi\;\xi^\alpha\phi(\xi,t). \quad \text{(B21)}$$

By Eqs. (B16), (B17), and (B12),

$$M_\alpha(t) = \frac{1}{6}\int dA\; A^{1+\alpha/6}\,\rho(A,t) = \frac{m_{n=1+\alpha/6}}{6}. \quad \text{(B22)}$$

Thus, in particular,

$$M_{\alpha=0}(t)=\frac{\Phi_A}{6}, \tag{B23}$$

$$M_{\alpha=-6}(t)=\frac{n_v(t)}{6}, \tag{B24}$$

$$M_{\alpha=3}(t)=\pi^{1/2}\Phi_V(t). \tag{B25}$$

By Eqs. (B22) and (B13),

$$\frac{dM_\alpha(t)}{dt}=\gamma f\left(-\frac{11}{6}-\frac{\alpha}{6}\right)M_{\alpha-1}. \tag{B26}$$

In particular, for $\alpha=0$ we have

$$\frac{dM_0(t)}{dt}=\gamma f\left(-\frac{11}{6}\right)M_{-1}(t). \tag{B27}$$

Equations (B27) and (B14) would yield the (expected) result $dM_0(t)/dt=0$ *provided* $M_{\alpha=-1}=m_{n=5/6}$ is *finite*. By Eq. (B21) with $\alpha=-1$, this is the case if $\phi(\xi,t)\to 0$ as $\xi\to 0$, or, by Eq. (B17), if $\rho(A)$ diverges no stronger than $1/A^{11/6}$ as $A\to 0$. Numerical results of Sec. III, Fig. 7, which indicate that $\rho(A)\sim 1/A^{11/6}$ [i.e., that $\phi(\xi=0,t)$ is a nonzero quantity], thus show that M_{-1} might be diverging. In these situations it would be wrong to equate the right-hand side of Eq. (B27) with zero. To discuss such a situation, let us consider Eq. (B26) in the limit $\alpha\to 0$. The right-hand side of Eq. (B26) can be expanded in powers of α as

$$\frac{dM_\alpha(t)}{dt}=-\gamma t\,\frac{\alpha}{6}\,f'\left(-\frac{11}{6}\right)M_{\alpha-1} \tag{B28}$$

to leading order in α. Furthermore, a partial integration of Eq. (B21) shows that

$$\alpha M_{\alpha-1}(t)=-\int_0^\infty d\xi\;\xi^\alpha\,\frac{\partial\phi(\xi,t)}{\partial\xi} \tag{B29}$$

for any positive α. By Eq. (B29), $\lim_{\alpha\to 0}[\alpha M_{\alpha-1}(t)]=\phi(\xi=0,t)$. Thus, by Eq. (B28),

$$\frac{dM_{\alpha=0}(t)}{dt}=-\frac{\gamma}{6}\,f'\left(-\frac{11}{6}\right)\phi(\xi=0,t). \tag{B30}$$

At first glance, Eq. (B30) violates conservation of the membrane area density. In fact, this equation is obtained by treating $\xi=A^{1/6}$ as a continuous variable on the interval $\xi>0$. In reality, however, $A>A_{\min}$, so $\xi>\xi_{\min}=A_{\min}^{1/6}$. Equation (B30) gives the rate with which the vesicles with $\xi>\xi_{\min}$ lose their membrane area density by producing the minimum-size vesicles with $\xi=\xi_{\min}$. In fact, the fissional production of the minimum size vesicles begins already at $t=0$, even for the initial monodisperse distribution $\rho(A)=n_0\delta(A-A_0)$, for which $\phi(\xi)=n_0A_0\delta(\xi-\xi_0)=6\Phi_A\delta(\xi-\xi_0)$, with $\xi_0=A_0^{1/6}$. By a simple calculation using Eq. (B18), we find that this monodisperse distribution first decays into a wedge-shaped intermediate distribution

$$\phi_{\rm int}\approx\frac{12\Phi_A}{\xi_0^2}\,\xi \tag{B31a}$$

for $\xi\ll\xi_0$, and

$$\phi_{\rm int}(\xi)=0 \tag{B31b}$$

for $\xi>\xi_0$. This $\phi_{\rm int}$ still has the same M_0 as the initial monodisperse distribution. However, by Eqs. (B20) and (B31a) we see that a nonzero $\phi(\xi=0)$ must develop in the evolution that follows. By Eq. (B30), this indicates onset of a strong fissional production of vesicles with $\xi=\xi_{\min}$. Eventually, all the vesicles would become minimum size vesicles. To qualitatively discuss how this happens, we use the fact that the fissional equation (B18) has an *exact* solution of the form

$$\phi(\xi,t)=a+b[\xi+\gamma f(-\tfrac{5}{3})t], \tag{B32}$$

where a and b are constants [as can be verified by Eqs. (B10) and (B14)]. For $t=0$, one has $\phi=a+b\xi$, which reduces (for $a=0$ and $b=12\Phi_A/\xi_0^2$) to the above $\phi_{\rm int}$, Eqs. (B31a) and (B31b), for the case of *infinite* ξ_0. This suggests that for $\xi\ll\xi(t)$, where $\xi(t)$ is the size of the largest vesicles [$\xi(t=0)=\xi_0$], one may approximate

$$\phi(\xi,t)\approx\frac{12\phi_A}{\xi_0^2}\,[\xi+\gamma f(-\tfrac{5}{3})t], \tag{B33a}$$

whereas

$$\phi(\xi,t)=0 \tag{B33b}$$

for $\xi>\xi(t)$. To find how the size of the largest vesicles $\xi(t)$ evolves with time, one can use Eq. (B30) and insert into it the approximate form of $\phi(\xi,t)$ in Eqs. (B33a) and (B33b). After some algebra, one obtains

$$\xi(t)\approx\xi_0-\gamma f(-\tfrac{5}{3})t, \tag{B34}$$

or, as $\xi=A^{1/6}$,

$$A(t)=A_0\left[1-\frac{t}{t_{\rm eq}}\right]^6, \tag{B35}$$

with

$$t_{\rm eq}=\frac{A_{\min}^{4/3}}{f(-\tfrac{5}{3})C\Gamma_0}\,A_0^{1/6}\sim R_0^{1/3}. \tag{B36}$$

Thus, the equilibration is dominated by the fissional decay of vesicles, which occurs in a *finite time* proportional to $R_0^{1/3}$, where R_0 is the initial vesicle size. During this decay, by Eqs. (B33), (B16), and (B17),

$$\rho(A,t)\approx\frac{12\Phi_A}{A_0^{1/3}}\,\frac{A^{1/6}+\gamma f(-\tfrac{5}{3})t}{A^{11/6}} \tag{B37}$$

for $A<A(t)$, and $\rho(A,t)=0$ for $A>A(t)$. Equation (B37) explains the transient behavior $\rho\sim A^{-11/6}$ observed in the numerical results discussed in Sec. III (see Fig. 7). The above results for $\rho(A,t)$ and $t_{\rm eq}$ are consequences of the particular form of the equilibrium vesicle distribution, Eq. (2.4) [which enters only the fissional part of the TE (2.1)]. Thus, they reflect the length scale dependence of membrane bending and saddle splay rigidity on the vesicle size [13], as well as entropy of vesicle's collective degrees of freedom incorporated in $\rho_{\rm eq}$ in Eq. (2.4) [5,6].

[1] *Statistical Mechanics of Membranes and Surfaces*, edited by D. R. Nelson, T. Piran, and S. Weinberg (World Scientific, Singapore, 1989).

[2] S. A. Safran, D. Roux, M. E. Cates, and D. Andelman, Phys. Rev. Lett. **57**, 491 (1986).

[3] L. Golubović and T. Lubensky, Phys. Rev. B **39**, 12 110 (1989).

[4] L. Golubović and T. Lubensky, Phys. Rev. A **41**, 4343 (1990).

[5] D. A. Huse and S. Leibler, J. Phys. (France) **49**, 605 (1988).

[6] D. Morse and S. Milner, Europhys. Lett. **26**, 565 (1994); Phys. Rev. E **52**, 5918 (1995). Our $\rho_{\rm eq}$ in Eq. (2.4) is identical to that of Refs. [5] and [6]. For convenience, here we express it in terms of the minimum-vesicle area $A_{\rm min}=4\pi R_{\rm min}^2$ rather than the surfactant molecular size a as in Refs. [5] and [6]. Consequently, our κ and $\overline{\kappa}$ really mean $\kappa(R_{\rm min})$ and $\overline{\kappa}(R_{\rm min})$ rather than $\kappa(a)$ and $\overline{\kappa}(a)$ as in Refs. [5] and [6]. In general, $R_{\rm min}>a$. For example, in the system studied experimentally in Ref. [12], $R_{\rm min}\approx 20$ nm. $R_{\rm min}$ is comparable to the upper size limit of membrane flakes; see M. Winterhalter and D. Lasić, Chem. Phys. Lipids **64**, 35 (1993).

[7] L. Golubović, Phys. Rev. E **50**, R2419 (1994).

[8] D. Morse, Phys. Rev. E **50**, R2423 (1994).

[9] *Liposomes in Biological Systems*, edited by G. Gregoriades and A. C. Allison (John Wiley, Chichester, 1980).

[10] *Liposome: From Physical Structure to Therapeutic Applications*, edited by C. K. Knight (Elsevier, Amsterdam, 1991). For methods to measure vesicle size distributions, see N. Ostrowsky, Chem. Phys. Lipids **64**, 45 (1993).

[11] *Liposome Technology*, edited by G. Gregoriades (CRC Press, Boca Raton, 1984).

[12] P. Hervè, D. Roux, A.-M. Bellocq, F. Nallet, and T. Gulik-Krzywicki, J. Phys. II **3**, 1255 (1993).

[13] See, F. David, in *Statistical Mechanics of Membranes and Surfaces* (Ref. [1]), p. 158.

[14] B. D. Simons and M. E. Cates, J. Phys. II **2**, 1439 (1992).

[15] L. V. Chernomordik and J. Zimmerberg, Current Opinion Struct. Biol. **5**, 541 (1995).

[16] Passage energy $E_{\rm pass}$ in *lamellar phases* has been discussed by Golubović [7], and de Vries [17]. For passages between vesicles the situation is similar but somewhat different in detail. Consider, for example, a passage connecting two nearby spherical vesicles having equal radius R. Such a membrane configuration can be obtained by removing two polar caps from the spheres and replacing them by catenoid connecting vesicles. (If the original spherical vesicles are sufficiently close, it is geometrically possible to *smoothly* connect them by a catenoid.) Passage energy $E_{\rm pass}$ can be then estimated from the standard Helfrich-Evans elastic model (1.1) yielding

$$E_{\rm pass}=-4\pi\overline{\kappa}-4\Omega\kappa.$$

Here the first term is the Gaussian curvature contribution evaluated by using Gauss-Bonnet theorem [it emerges due to change of membrane topology that occurs during vesicle fusion; see, e.g., W. Harbich, R. M. Servus, and W. Helfrich, Z. Naturforsch. A **33**, 1013 (1978)]. The second term in $E_{\rm pass}$ is the mean curvature contribution. Here Ω is the solid angle subtended by each of the polar caps (from the geometrical condition that the catenoid with the neck radius $R_{\rm neck}$ is smoothly connected to the two spheres, we find $\Omega\approx\pi R_{\rm neck}/R$, for $R_{\rm neck}\ll R$). Interestingly, for $\kappa>0$, the mean curvature contribution to $E_{\rm pass}$ is *negative* here, as the curved polar caps are replaced by a piece of catenoid that is a minimal, zero mean curvature surface. This mean curvature effect would energetically *favor* passage creation. However, for a small passage just emerging from a vesicle fusion $R_{\rm neck}\ll R$, and the solid angle Ω is small. Thus, if $\kappa\sim\overline{\kappa}$, one can ignore the mean curvature contribution to $E_{\rm pass}$. So, within the standard Helfrich-Evans model (1.1) one finds $E_{\rm pass}\approx-4\pi\overline{\kappa}$, i.e., $E_{\rm pass}\approx 4\pi|\overline{\kappa}|$ for $\overline{\kappa}<0$. The standard Helfrich-Evans model (1.1), however, ignores higher order terms in powers of curvature [17], which are important here as the neck radius of a passage just emerging from vesicle fusion is small ($R_{\rm neck}\sim R_{\rm min}$, where $R_{\rm min}$ is the radius of the minimum size vesicles with the area $A_{\rm min}=4\pi R_{\rm min}^2$]. These higher order curvature terms yield passage energy corrections that are typically positive and of the order κ for $R_{\rm neck}\sim R_{\rm min}$ [17]. Thus, for passages emerging from vesicle fusions, $E_{\rm pass}>4\pi|\overline{\kappa}|$ for $\overline{\kappa}<0$.

[17] M. D. Mitov, C. R. Acad. Bulg. Sci. **31**, 513 (1978); R. de Vries, J. Chem. Phys. **103**, 6740 (1995).

[18] Roughly, $\Phi_{A,\rm cvc}/\Phi_{A,\rm clvc}\approx\exp\{-[E_{\rm agg}-E(A_{\rm min})]/k_BT\}$, where $E_{\rm agg}$ is the bilayer aggregation energy (binding energy) per surfactant molecule and $E(A_{\rm min})=8\pi\kappa+4\pi\overline{\kappa}$ is the curvature energy of minimum size vesicle. Generally, $E_{\rm agg}$ is (at least) a few times larger than $E(A_{\rm min})$. Thus, generally, $\Phi_{A,\rm cvc}<\Phi_{A,\rm clvc}$.